Influence of He^{++} and shock geometry on interplanetary shocks in the solar wind: 2D Hybrid simulations

L. Preisser[1], X. Blanco-Cano[1], D. Trotta[2], D. Burgess[2], P. Kajdič[1]

[1]Instituto de Geofísica, UNAM, Mexico City

[2]School of Physics and Astronomy, QMUL, London

Corresponding author: preisser@igeofisica.unam.mx

EGU-Online General Asembly, May 2020

Just published in JGR, please click
https://doi.org/10.1029/2019JA027442

Outline

Motivation & Summary

- Alpha particles (He^{++}) constitute typically about 5% of SW.
- Different charge-to-mass ratio H^+ and He^{++} $\Rightarrow$ Different acceleration at shocks.
- $\Rightarrow$ Changes in the VDFs for both species.
- $\Rightarrow A = T_\perp / T_\| > 1$ (considered to be the energy source for Mirror/IC waves for instance)
- But... How $T_\perp / T_\|$ and shock structure depend on the percentage of He^{++} and θ_{Bn} is not well understood.
- We have performed various 2.5-D local hybrid simulations of IP-shock varying the initial θ_{Bn} and He^{++} percentage.
- We have found changes in the shock transition behavior as well as in temperature anisotropy as functions of both the shock geometry and He^{++} particle abundance.
- Change in θ_{Bn} leads to variations of the efficiency with which particles can escape to the upstream region facilitating or not the formation of compressive structures in the magnetic field that will produce increments in perpendicular temperature.

Simulation Setup

- 2.5-D hybrid (kinetic ions/fluid electrons) simulations using HYPSI code.
- Spatial and temporal scales in units of $d_i = c/\omega_p$ and Ω_p^{-1} respectively.
- $n_x \times n_y = 1000 \times 800$ with cell sizes $\Delta x = \Delta y = 0.5\ c/\omega_p$
- **V**, **B** and **E** field vectors including all 3D components.
- Δt was chosen so that $\Omega_p \Delta t = 0.005$
- Initially $V_{in} = 3.3\ V_A$ along x with **B** in x-y plane
- Upstream H^+ and He^{++} with Maxwellian VDF and $\beta = 0.5$
- We perform different runs with initial $\theta_{Bn} = 15°, 30°, 50°, 65°$
- For each θ_{Bn} we vary the relative number density fraction of He^{++} i.e. $n_\alpha / n_p = 0.01, 0.05, 0.10$
- We perform a total of 12 simulations (see Figure 1).

Simulation Results: Magnetic Field

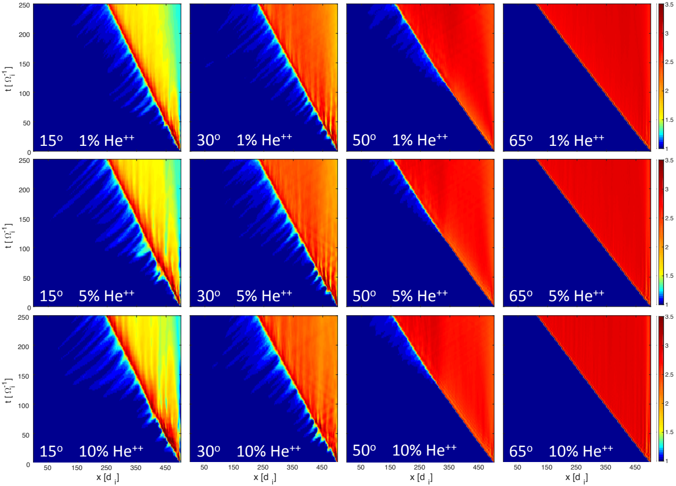

Figure 1: Figure matrix showing the time evolution of total magnetic field (averaged over y-axis) for all the runs in this work. θ_{Bn} increases from left to right while the He^{++} number density fraction increases from top to bottom. The change in color from navy to aqua occurs at **B** $\sim$1.25 while the change from green to yellow occurs at **B** $\sim$ 1.5.

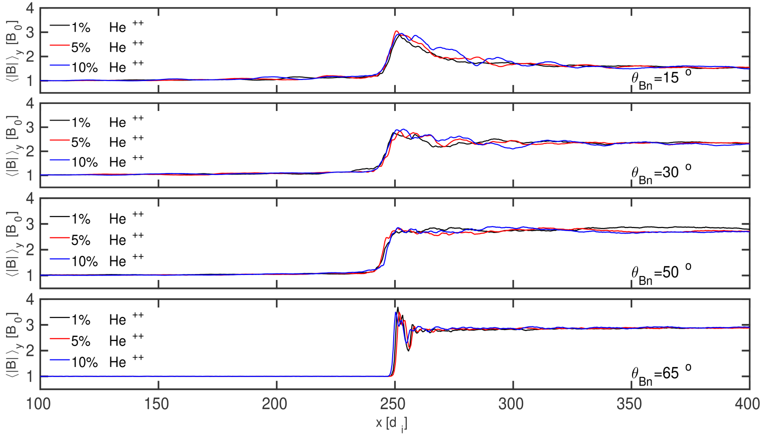

Figure 2: Total magnetic field profile (average over y-axis) for the all the different θ_{Bn} values used in this work when the shock arrives to $\sim 250\ d_i$. The θ_{Bn} angle increases from top to bottom, He^{++} number density fraction is indicated by different colors (black: 1%, red: 5%, blue: 10%).

Simulation Results: Temperature Anisotropy

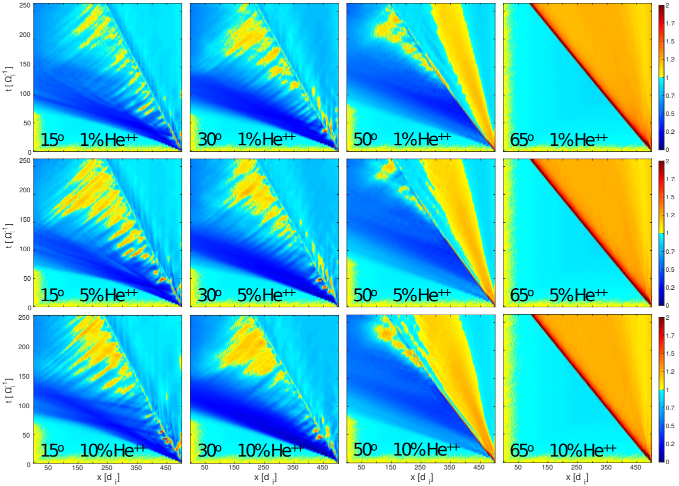

Figure 3: Figure matrix showing the time evolution of temperature anisotropy for protons (averaged over y-axis) for all the runs in this work. θ_{Bn} increases from left to right while the He^{++} number density fraction increases from top to bottom. The color palette is chosen to show anisotropy values less (in blue) and greater (in yellow-red) than 1.

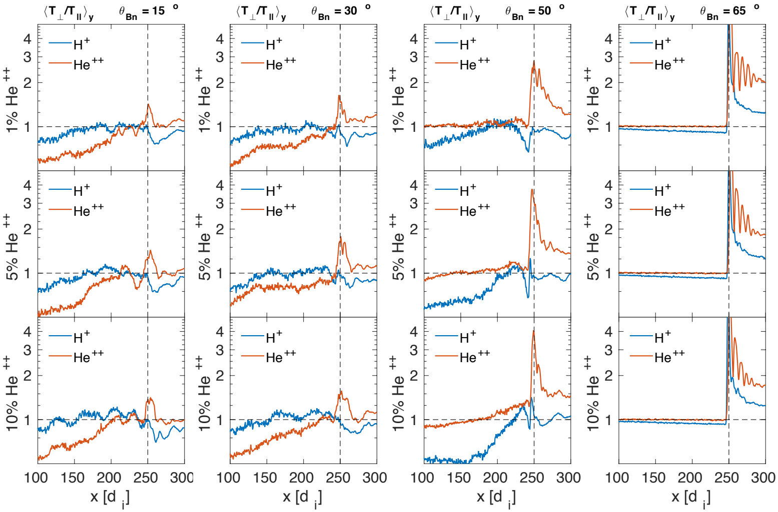

Figure 4: Semi-log temperature anisotropy profiles (average over y-axis) for protons (blue) and He^{++} (orange) at the time when the shock arrives to $\sim 250\ d_i$ for all the θ_{Bn} values and He^{++} percentages in this work. The vertical dashed line indicates the shock localization and the horizontal dashed line indicates $T_\perp / T_\parallel = 1$

Simulation Results: VDFs

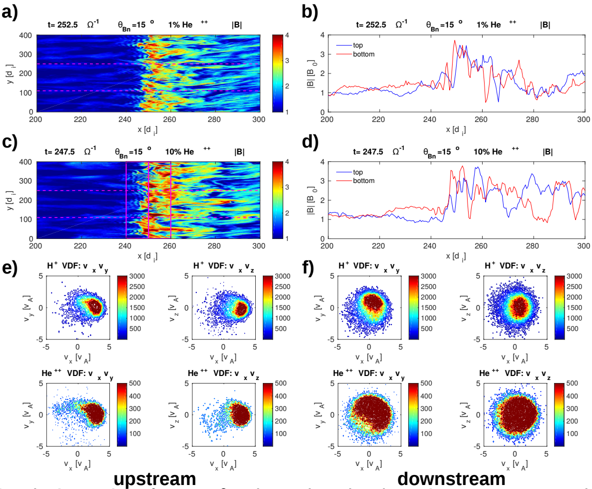

Figure 5: Simulation with θ_{Bn}=15° when the shock arrives to x=250 d_i: a) **B** and b) **B** along two cuts at upper (blue) and lower (red) dashed lines in panel a) for case with 1% of He^{++}. Panels c) and d) show the same results for case with 10% of He^{++}. VDF's for both species for the case with 10% of He^{++} contained inside the left (upstream) magenta box on panel c) are shown in panels e). The same results for the right (downstream) magenta box on panel c) are shown in panels f).

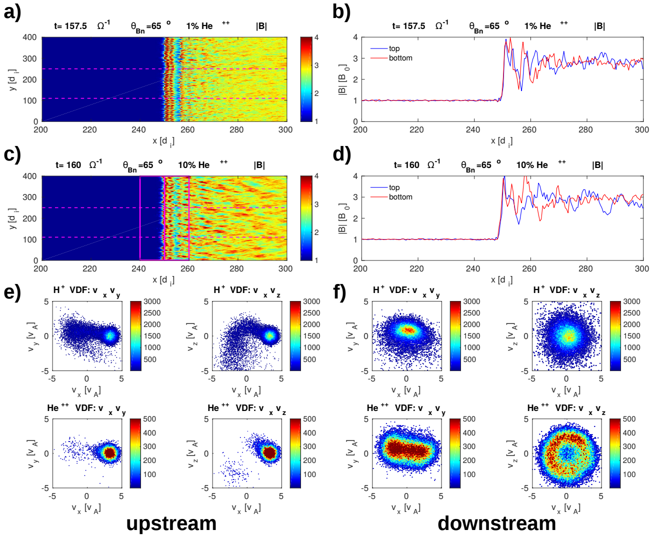

Figure 6: Simulation with θ_{Bn}=65° when the shock arrives to x=250 d_i: a) **B** and b) **B** along two cuts at upper (blue) and lower (red) dashed lines in panel a) for case with 1% of He^{++}. Panels c) and d) show the same results for case with 10% of He^{++}. VDF's for both species for the case with 10% of He^{++} contained inside the left (upstream) magenta box on panel c) are shown in panels e). The same results for the right (downstream) magenta box on panel c) are shown in panels f).

Simulation Results: Density Behavior

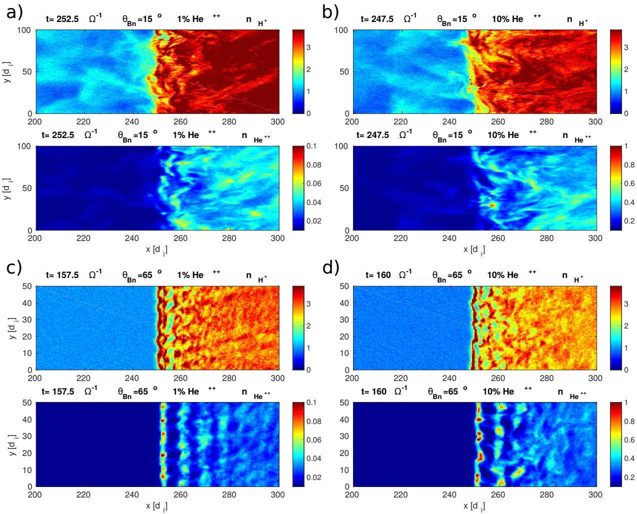

Figure 7: Contour plots of protons and He^{++} densities corresponding to the simulations with $\theta_{Bn} = 15^\circ$ for a) 1% and b) 10% of He^{++} and with $\theta_{Bn} = 65^\circ$ for c) 1% and d) 10% of He^{++}. The time of the plots correspond to those magnetic field magnitude plots in Figures 5 and 6.

Simulation Results: Mirror Mode and IC Instability

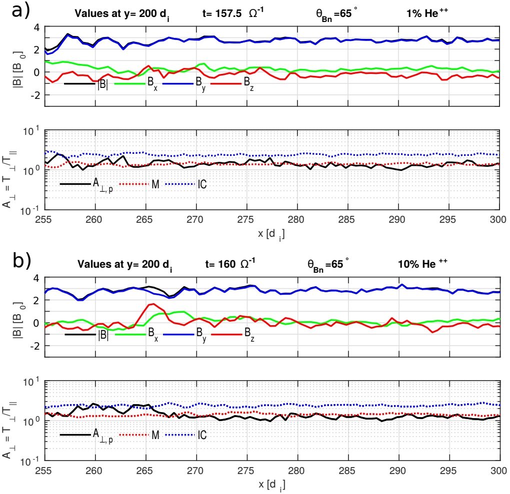

Figure 8: **B**-field and A_p along downstream region at $y = 200\ d_i$ for simulations with $\theta_{Bn} = 65^\circ$ and a) 1% and b) 10% of He^{++}. A_p and the parameters M$= 1+1/\beta_\perp$ (red) and IC$= 1 + \beta_\parallel^{0.5}$ (blue) are shown in bottom panels. The condition for the growing of the mirror instability is fulfilled by the threshold $T_\perp/T_\parallel > \mathrm{M}$, the condition for ion/cyclotron instability is $T_\perp/T_\parallel < \mathrm{IC}$. The plots time are the same as in Figure 7.

Conclusions

- We have shown with the help of hybrid simulations that both, geometry and He^{++} content can modify the interplanetary shock profile and the the upstream and downstream characteristics affecting $T_{\perp}/T_{\parallel}$, VDFs properties and $\delta\mathbf{B}$ growth.
- Variation of θ_{Bn} changes the efficiency with which particles can escape to the upstream side of the shock influencing the formation of compressive structures and the $\mathbf{B}$ profile.
- $\mathbf{B}$ profile is affected by θ_{Bn}: $\mathbf{B}$ jump at shock is more abrupt as θ_{Bn} increases, while $\delta\mathbf{B}$ is attenuated as as θ_{Bn} increases.
- $A_{p,\alpha}$ depend on θ_{Bn}: For 15°, 30°, $A_{\alpha} < A_p$ upstream and $A_{\alpha} > A_p$ downstream. For 50° $A_{\alpha} > A_p$. For 65°, $A_{p,\alpha} \sim 1$ upstream and $A_{\alpha} > A_p$ downstream. An A_{α} peak is formed at shock transition ($\forall\ \theta_{Bn}$) tending to be larger as θ_{Bn} increases.
- VDFs are affected by θ_{Bn}: For 15° backstreaming H^{+} and He^{++} are observed upstream in contrast with the 65° case. An He^{++} ring-like distribution is formed downstream. Downstream VDFs for H^{+} are more isotropic and thermalized for 15° than for the 65° case.

- He^{++} content affects $\mathbf{B}$ profile: As He^{++} increase compressive $\delta\mathbf{B}$ on both sides of the shock reach higher amplitudes for 15°, 30°. For 50°, the He^{++} content does not affect their amplitude. For 65° downstream $\delta\mathbf{B}$ reach larger amplitudes as He^{++} increases.
- Upstream zones where $A_p > 1$ coincide with those with compressive $\delta\mathbf{B}$. For the quasi-parallel cases (15°, 30°) upstream zones with $A_p > 1$ are less fragmented as He^{++} content increases. For 50° this behavior is repeated. Comparing A_p and A_α the He^{++} content does not affect the peak shape at shock for 15°, 30° cases. For 50° an increment is observed as He^{++} increases. For 65° the peak decreases as He^{++} increases.
- He^{++} content affects the VDF distributions making them more spread as He^{++} increases in both quasi-parallel and quasi-perpendicular cases.

Acknowledgements

We thank Dirección General de Cómputo y de Tecnologías de Información y Comunicación (DGTIC) of the Universidad Nacional Autónoma de México (UNAM) for the allocation and support received in the use of the HP Cluster Platform 3000SL supercomputer (MIZTLI). Contract grant sponsor: DGTIC-UNAM resources (project LANCAD-UNAM-DGTIC-337). The authors acknowledge support from the Royal Society Newton International Exchange Scheme (Mexico) grant NI150051. L.P. thanks CONACYT becas nacionales 2015-2019 grant 174700. X. B. C. is supported by CONACyT grant (255203) and DGAPA project (IN105218-3). D. B. was supported by the UK Science and Technology Facilities Council (STFC) grant ST/P000622/1. D.T. acknowledges support of a studentship funded by the Perren Fund of the University of London. P.K. is supported by PAPIIT grant (IA101118).